Problems in Modeling UWB Channels

Robert A. Scholtz and Joon-Yong Lee

Abstract— **Ultrawideband (UWB) channel models pose a new set of problems to the designer. The very wide radio-frequency bandwidth employed by a UWB radio means that more structure of the channel is exposed by the fine time-resolution of the UWB radio receiver. Issues pertinent to design and simulation of UWB communication and ranging systems will be illustrated through a set of UWB measurements.**

I. Introduction

THE inherent time resolution (or range resolution) of a signal $s(t)$ can be determined by evaluating the response of a matched filter detector to small time displacements τ of $s(t)$. The ambiguity function provides a plot of the detector output as a function of τ that has a peak at $\tau = 0$, the response when there is no timing error. The width of this peak, which is a measure of time resolution, is inversely proportional to the bandwidth, and hence is very small for ultrawideband signals. Woodward's radar ambiguity function [5] for narrowband signals has two parameters: time mismatch τ and frequency mismatch to account for unknown doppler shifts and oscillator offsets. For a carrierless UWB signal, a similar ambiguity function is defined using time mismatch τ and time-scaling factor α (related to clock offset), this scaling being the source of doppler shift in narrowband signals. It is important that the stability of clocks in UWB systems be good enough to insure that clock jitter is significantly smaller than the resolution of the receiver's detector.

Ranging to the full theoretical capabilities of UWB signals is not a simple task. As bandwidth increases, a single multipath component at low bandwidth may be time-resolved into multiple components, usually each with a smaller level of energy content. Ranging requires that the direct path portion of the signal be located and its arrival time inserted into ranging algorithms. Finding the direct path component among possibly hundreds of resolvable multipath components is signal-processing intensive, especially since the direct path, while earliest in arrival time, may be considerably smaller in amplitude than later arriving components [2], [4]. A time-of-arrival (ToA) measurement algorithm for UWB ranging, which assumes the presence of over-sampled measurement data, was introduced in [4]. In this paper, we suggest a modification of the ToA algorithm to reduce the number of correlation computations (samples) in the direct-path search process, thereby reducing the time to produce a range estimate.

This work was supported by the Office of Naval Research under Contract No. N00014-00-0221.

Robert Scholtz is with the University of Southern California, Los Angeles, CA 90089-2565. e-mail: scholtz@usc.edu.

Joon-Yong Lee is with Handong Global University, Pohang, Korea. e-mail: joonlee@handong.edu.

II. UWB Ambiguity Function

A. Definition

Let's assume that a UWB time-limited signal is transmitted through a free-space channel. Ignoring receiver noise, the received signal $s_{\rm r}(t)$ is of the form

$$s_{\rm r}(t) = A_{\rm r} s\Big(\alpha(t-\tau_{\rm r})\Big), \tag{1}$$

where $A_{\rm r}$ is the amplitude of received signal, $\tau_{\rm r}$ is an time-shift, and α is a time-scale factor. The receiver, not having prior knowledge of $A_{\rm r}$, $\tau_{\rm r}$, and α, constructs a matched-filter/correlator matched to $s_{\rm m}(t)$, which is

$$s_{\rm m}(t) = A_{\rm m} s(t-\tau_{\rm m}), \tag{2}$$

and the matched filter output $z(t)$ is given by

$$\begin{aligned} z(t) &= A_{\rm r}A_{\rm m}\int_{-\infty}^{\infty} s(t-\tau_{\rm m}) s\Big(\alpha(t-\tau_{\rm r})\Big)dt \\ &= \frac{A_{\rm r}A_{\rm m}}{\sqrt{\alpha}}\int_{-\infty}^{\infty}\sqrt{\alpha}s(t)s\Big(\alpha(t-\tau)\Big)dt \end{aligned} \tag{3}$$

where

$$\tau = \tau_{\rm r} - \tau_{\rm m}. \tag{4}$$

The UWB ambiguity function, namely $\chi_{\rm uwb}(\tau,\alpha)$, can be defined as

$$\chi_{\rm uwb}(\tau,\alpha) = \int_{-\infty}^{\infty}\sqrt{\alpha}s(t)s(\alpha(t-\tau))dt, \tag{5}$$

where $\sqrt{\alpha}$ is for normalization so that the signal energy is kept constant. The UWB ambiguity function satisfies

$$\chi_{\rm uwb}(\tau,\alpha) \le \chi_{\rm u}(0,1) = E_{\rm s}, \tag{6}$$

where $E_{\rm s}$ denotes the energy of $s(t)$,

$$E_{\rm s} = \int_{-\infty}^{\infty}|s(t)|^2dt = \int_{-\infty}^{\infty}|S(f)|^2df, \tag{7}$$

where $S(f)$ is the Fourier transform of $s(t)$. If α is equal to 1, $\chi_{\rm uwb}(\tau,\alpha)$ can be interpreted as the auto-correlation function of $s(t)$.

The function $\chi_{\rm uwb}(\tau,\alpha)$ can be approximated near $(0,1)$ using the initial terms of a Taylor series expansion.

$$\begin{aligned} \chi_{\rm uwb}(\tau,\alpha) \approx \chi_{\rm uwb}(0,1)\Big[1 + A_\tau\tau + A_\alpha(\alpha-1) + \frac{1}{2}B_\tau\tau^2 \\ + \frac{1}{2}B_\alpha(\alpha-1)^2 + \frac{1}{2}B_{\tau\alpha}\tau(\alpha-1)\Big], \end{aligned} \tag{8}$$

where A_τ, A_α, B_τ, B_α, and $B_{\tau\alpha}$ are defined as

$$\begin{cases} A_\tau &= \dfrac{1}{\chi_{\rm uwb}(0,1)}\dfrac{\partial}{\partial\tau}\chi_{\rm u}(\tau,\alpha)\Big|_{\tau=0,\alpha=1}, \\ A_\alpha &= \dfrac{1}{\chi_{\rm u}(0,1)}\dfrac{\partial}{\partial\alpha}\chi_{\rm uwb}(\tau,\alpha)\Big|_{\tau=0,\alpha=1}, \\ B_\tau &= \dfrac{1}{\chi_{\rm u}(0,1)}\dfrac{\partial^2}{\partial\tau^2}\chi_{\rm uwb}(\tau,\alpha)\Big|_{\tau=0,\alpha=1}, \\ B_\alpha &= \dfrac{1}{\chi_{\rm u}(0,1)}\dfrac{\partial^2}{\partial\alpha^2}\chi_{\rm uwb}(\tau,\alpha)\Big|_{\tau=0,\alpha=1}, \\ B_{\tau\alpha} &= \dfrac{1}{\chi_{\rm u}(0,1)}\dfrac{\partial^2}{\partial\tau\partial\alpha}\chi_{\rm uwb}(\tau,\alpha)\Big|_{\tau=0,\alpha=1}. \end{cases} \tag{9}$$

and evaluated by

$$A_\tau = A_\alpha = 0, \tag{10}$$

$$B_\tau = -\frac{1}{\chi_{\rm uwb}(0,1)}\int_{-\infty}^{\infty}(2\pi f)^2|S(f)|^2 df, \tag{11}$$

$$B_\alpha = \frac{1}{\chi_{\rm uwb}(0,1)}\left[-\frac{3E_{\rm s}}{4}+\int_{-\infty}^{\infty}t^2 s(t)s''(t)dt\right], \tag{12}$$

$$B_{\tau\alpha} = -\frac{1}{\chi_{\rm uwb}(0,1)}\int_{-\infty}^{\infty}ts(t)s''(t)dt. \tag{13}$$

Using the fact that $E_{\rm s}/\chi_{\rm uwb}(0,1)$ integrates to 1, we can relate the Gabor (or rms) bandwidth $B_{\rm rms}$ (in Hertz) of the signal $s(t)$ to B_τ by

$$\frac{B_\tau^{\frac{1}{2}}}{2\pi} = B_{\rm rms} = \left[\int_{-\infty}^{\infty}f^2\frac{|S(f)|^2}{\chi_{\rm u}(0,1)}df\right]^{\frac{1}{2}}. \tag{14}$$

This large value of B_τ for UWB signals makes the shape of the peak of $\chi(\tau,\alpha)$ very narrow as a function of time, thereby justifying the fine time resolution capability of a matched UWB receiver.

B. Computer Plots

UWB ambiguity functions with different formats were evaluated using computer simulations. In these simulations, the received UWB pulse $s(t)$ was assumed to be the second derivative of a gaussian shape, which is given by [3]

$$s(t) = \Big[1-4\pi(t/\tau_m)^2\Big]\exp\Big[-2\pi(t/\tau_m)^2\Big], \tag{15}$$

where $\tau_m = 0.781\times10^{-9}$.

Figure 1 shows the ambiguity function of a single UWB pulse. The range of the scale factor α goes well beyond mismatches that which can be caused by radial velocities by transmitter and receiver, and hence the velocity resolution is not very good, while the time resolution is very fine. This ambiguity function of a single UWB pulse can be classified as the knife-edge type.

Suppose the UWB ranging system transmits and receives a train of pulses. Because of the absence of a common clock, there may exist mismatch in the clock periods of the

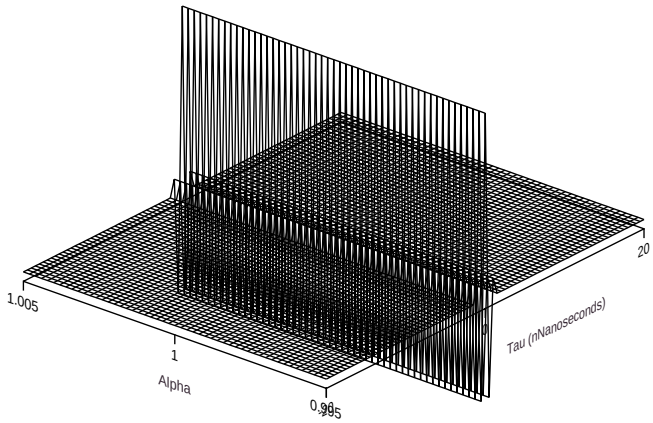

Fig. 1. UWB ambiguity function of a single pulse.

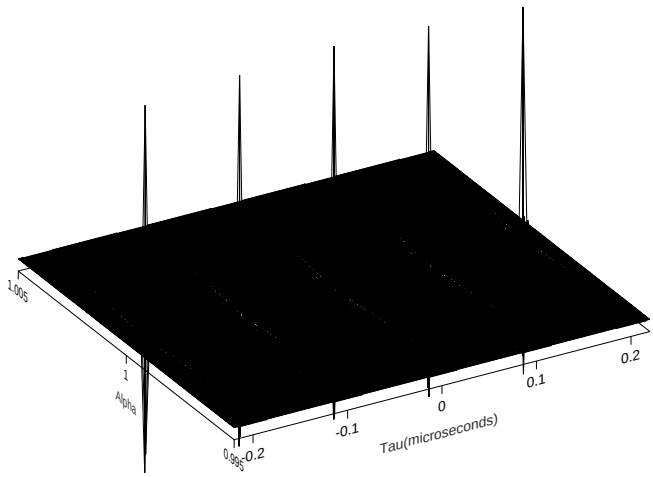

Fig. 2. UWB ambiguity function of a periodic train of 64 pulses. The pulse repetition rate is 10 Mpps.

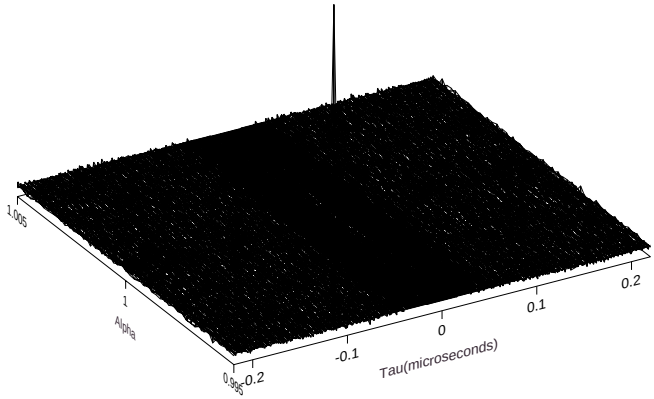

Fig. 3. UWB ambiguity function of 64 time hopped pulses with $N_{\rm h} = 32$, $T_{\rm f} = 100$ ns, and $T_{\rm c} = 2$ ns.

transmitter and receiver. The order of the clock period mismatch can be possibly as large as 0.1% for a very poor clock. Let's assume no pulse-shape distortion, but instead consider the clock period mismatch as the second factor of the UWB ambiguity function. In this case the UWB ambiguity function of a train of N_{p} periodic pulses can be computed as

$$\chi_{\mathrm{u}}(\tau,\alpha)=\int_{-\infty}^{\infty}\sum_{i=0}^{N_{\mathrm{p}}-1}\sum_{j=0}^{N_{\mathrm{p}}-1}s\left(t-iT_{\mathrm{f}}+\frac{(N_{\mathrm{p}}-1)T_{\mathrm{f}}}{2}\right)\cdot s\left(t-\tau-j\alpha T_{\mathrm{f}}+\frac{(N_{\mathrm{p}}-1)T_{\mathrm{f}}}{2}\right)dt, \quad (16)$$

where T_{f} is the clock period and α is the scaling factor caused by clock period differences, which is equal to

$$\alpha=\frac{T_{\mathrm{f}}}{T_{\mathrm{f}}+T_{\mathrm{d}}}, \quad (17)$$

where T_{d} denotes the clock period mismatch. Detailed evaluation of the ambiguity function of the periodic gaussian pulse train is given in [6] and figure 2 is a simulated ambiguity function. The number of pulses was assumed to be 64 and pulse repetition rate is 10 Mpps. We can still measure the range with a fine resolution but with a pulse-repetition-time ambiguity in time mismatch. Figure 3 is the ambiguity function of a train of time hopped pulses, which is represented by

$$\chi_{\mathrm{u}}(\tau,\alpha)=\int_{-\infty}^{\infty}\sum_{i=0}^{N_{\mathrm{p}}-1}\sum_{j=0}^{N_{\mathrm{p}}-1}s\left(t-iT_{\mathrm{f}}-c_i(u)T_{\mathrm{c}}+\frac{(N_{\mathrm{p}}-1)T_{\mathrm{f}}}{2}\right)\cdot s\left(t-j\alpha T_{\mathrm{f}}-c_j(u)T_{\mathrm{c}}+\frac{(N_{\mathrm{p}}-1)T_{\mathrm{f}}}{2}\right)dt, \quad (18)$$

where T_{f} and T_{c} denote frame time and chip time, respectively. The time hopping sequence $\{c_j(u)\}$ satisfies

$$0\le c_i(u)\le N_h-1. \quad (19)$$

It was assumed that $N_{\mathrm{p}}=64$, $N_{\mathrm{h}}=32$, $T_{\mathrm{f}}=100$ ns, and $T_{\mathrm{c}}=2$ ns. The time-hopping pattern of the sequence employed here was assumed to be uniform over 32 time bins. Notice that ambiguities along time axis were suppressed down by time-hopping.

III. A System-Friendly Algorithm for UWB Ranging

A. Modification of the ToA Algorithm

The ToA measurement algorithm using generalized maximum likelihood estimation (GML) was introduced in [4]. In this algorithm, the ToA of the direct path signal is estimated using two critical parameters, relative strength and relative time displacement between the strongest path and the potential direct path signal, with over-sampled measurement data. However, in real systems, the measurement time is limited and the sampling frequency may not be high enough to perform the GML estimation.

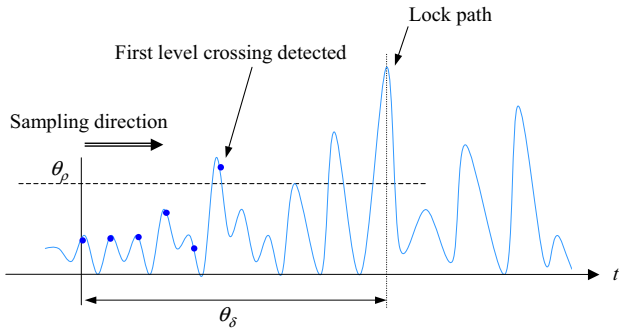

Fig. 4. Search for the earliest arrival of the signal using uniform sampling. Search is performed in a positive direction along the time axis.

The ToA algorithm can be modified in a system-friendly manner as follows. First, the search region for the direct path signal with a given length of θ_δ is set in the forward direction from the location of the locked path instead of the strongest path to reduce the measurement time spent on the peak search. It is difficult to characterize the time displacement between the locked path and the strongest path without a thorough knowledge of the acquisition scheme. However, considering that the acquisition strategy is based on threshold detection, by which the tracking correlator is locked on the first level crossing point at the threshold, we can assume that the correlator is locked on a path which arrives earlier than the peak path. As a consequence, the probability of a false detection in the noise only portion of the signal would increase, while the risk of missing the direct path signal beyond the range of search would decrease. Secondly, the threshold of the amplitude (θ_ρ) is determined only by the noise floor without considering the relative path strength due to the absence of the knowledge of the peak strength. Thirdly, the first level crossing point is regarded as the ToA of direct path signal since computation of GML estimation cannot be done with under-sampled data.

Figure 4 illustrates the search process. Search by sampling is done in the positive direction along the time axis and terminated once the first level crossing is detected.

B. Sampling Issues

To achieve an accurate detection in a limited measurement time, which is determined by sampling rate, length of search region, and the number of pulse periods per measurement, effective sampling design is critical. To determine the sampling strategy, it is necessary to know the minimum sampling frequency required. For example, the larger the distance between two adjacent samples, the higher is the risk of missing the level crossing point between them.

While it is very difficult to evaluate the probability of missing a level crossing between samples, we can think of some ways to measure this risk. One of them is to quantify the interpolation error caused by under-sampling, assuming the signal is deterministic. Since the signal from which

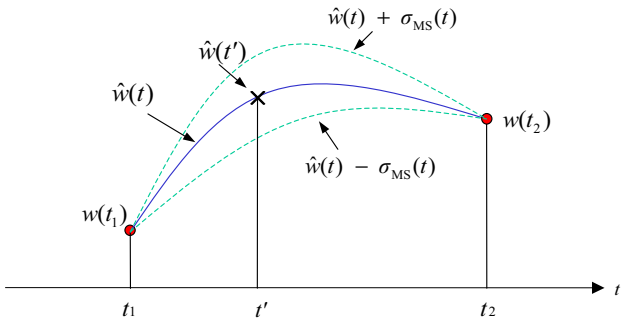

Fig. 5. Reconstruction of signal using MMSE estimation based on two samples. Solid curve indicates the reconstructed signal and the dotted line shows the error deviation.

the samples are taken is not band-limited, it is impossible to sample at the Nyquist rate and as a consequence, perfect signal reconstruction from samples is impossible [7]. The amount of energy in high frequency signal components lost due to aliasing will provide one way of measuring the sampling quality. Another approach is to evaluate the error variance in minimum mean square error (MMSE) estimation, assuming the correlator output signal is a wide sense stationary process. Figure 5 shows an example of MMSE estimation using two samples. In this figure, $\hat{w}(t')$ denotes the MMSE estimate of $w(t')$ evaluated with observation vector of samples, namely $\underline{m}$, which is

$$\underline{m} = \begin{bmatrix} w(t_1) \\ w(t_2) \end{bmatrix}. \tag{20}$$

The solid line represents the reconstructed signal using MMSE estimation and the dotted lines represent one standard deviation of the estimation error. The closer the dotted line is to the threshold level at which the crossing is searched, the larger is the probability of missing the occurrence of a threshold crossing. MMSE estimate of $w(t')$ and the error variance $\sigma^2_{\mathrm{MS}}(t')$ are given by

$$\hat{w}(t') = R_{\hat{\mathrm{w}}\mathrm{m}} R_{\mathrm{m}}^{-1} \underline{m}, \tag{21}$$
$$\sigma^2_{\mathrm{MS}}(t') = \mathrm{Tr}\big(R_{\hat{\mathrm{w}}} - R_{\hat{\mathrm{w}}\mathrm{m}} R_{\mathrm{m}}^{-1} R_{\mathrm{m}\hat{\mathrm{w}}}\big), \tag{22}$$

where $R_{\hat{\mathrm{w}}}$ and R_{m} are correlation matrix $\hat{w}(t')$ and $\underline{m}$, respectively, $R_{\hat{\mathrm{w}}\mathrm{m}}$ is the cross-correlation matrix of $\hat{w}(t')$ and $\underline{m}$, and $\mathrm{Tr}(\cdot)$ is the trace function. Correlation matrices appearing in (21) are evaluated by computing

$$R_{\hat{\mathrm{w}}} = R_{\mathrm{w}}(0), \tag{23}$$
$$R_{\mathrm{m}} = \begin{bmatrix} R_{\mathrm{w}}(0) & R_{\mathrm{w}}(t_1 - t_2) \\ R_{\mathrm{w}}(t_2 - t_1) & R_{\mathrm{w}}(0) \end{bmatrix}, \tag{24}$$
$$R_{\hat{w}m} = [R_{\mathrm{w}}(t' - t_1)\ R_{\mathrm{w}}(t' - t_2)], \tag{25}$$

where $R_{\mathrm{w}}(\tau)$ denotes the auto-correlation function of $w(t)$. As shown in (21) through (25), to calculate $\hat{w}(t')$ and $\sigma^2_{\mathrm{MS}}(t')$, auto-correlation function of the correlator output signal must be evaluated.

Figure 6 is the block diagram of a matched filter system which is equivalent to a potential UWB radio link. A

Fig. 6. Transmission and reception of signal in UWB radio link.

transmitted UWB pulse $p(t)$ goes though the channel including antennas whose impulse response is $h_{\mathrm{b}}(t)$, and the resulting output is correlated/match-filtered with the template signal $u(t)$. Assuming the correlator output $w(t)$ is a wide sense stationary random process, the energy spectral density $S_{\mathrm{w}}(f)$ of $w(t)$ can be approximated by

$$S_{\mathrm{w}}(f) = |U(f)|^2 |H_{\mathrm{b}}(f)|^2 S_{\mathrm{p}}(f), \tag{26}$$

where $S_{\mathrm{p}}(f)$ is the energy spectral density of $p(t)$. The channel function $H_{\mathrm{b}}(f)$ can be modeled using the measured antenna system function $H_{\mathrm{a}}(f)$ shown in figure 8, which is

$$H_{\mathrm{b}}(f) = c_{\mathrm{a}} \cdot H_{\mathrm{a}}(f), \tag{27}$$

where the unknown constant c_{a} is the attenuation factor. The antenna system measurement to evaluate $H_{\mathrm{a}}(f)$ is given in [1]. Let's define $S'_{\mathrm{w}}(f)$ and $R'_{\mathrm{w}}(\tau)$ as

$$S'_{\mathrm{w}}(f) = |U(f)|^2 |H_{\mathrm{a}}(f)|^2 S_{\mathrm{p}}(f), \tag{28}$$
$$R'_{\mathrm{w}}(\tau) = F^{-1}\{S'_{\mathrm{w}}(f)\}. \tag{29}$$

Then, $S_{\mathrm{w}}(f)$ and $R_{\mathrm{w}}(\tau)$ satisfy

$$S_{\mathrm{w}}(f) = c_{\mathrm{a}}^2 \cdot S'_{\mathrm{w}}(f), \tag{30}$$
$$R_{\mathrm{w}}(\tau) = c_{\mathrm{a}}^2 \cdot R'_{\mathrm{w}}(\tau). \tag{31}$$

In figure 7 through figure 10, plots of $S_{\mathrm{p}}(f)$, $|U(f)|^2$, $S'_{\mathrm{w}}(f)$, and $R'_{\mathrm{w}}(\tau)$ are shown. Again, the template $u(t)$ is the second derivative of a gaussian pulse as shown in (15). The unknown constant c_{a} can be evaluated using (31), which is

$$c_{\mathrm{a}} = \sqrt{\frac{R_{\mathrm{w}}(0)}{R'_{\mathrm{w}}(0)}} = \sqrt{\frac{E_{\mathrm{w}}}{R'_{\mathrm{w}}(0)}}, \tag{32}$$

where E_{w} is the total energy of $w(t)$. So calculation of c_{a} requires knowledge of the total energy of $w(t)$, which is difficult to estimate without knowledge of the channel.

Figure 11 and figure 12 are examples of the standard deviation of error, $\sigma_{\mathrm{MS}}(t)$, assuming c_{a} is equal to 1. Figure 11 compares $\sigma_{\mathrm{MS}}(t)$ with different sampling rates, assuming the number of samples used for the estimation is 2. Notice that the peak of each curve is located at the midpoint between the two samples. Figure 12 shows another comparison of $\sigma_{\mathrm{MS}}(t)$ with a different number of observations used for the estimation, while the sampling rate is fixed at 2 GHz, assuming the closest samples are used for estimation. The error deviation decreases as the number of observations used increases.

IV. Conclusions

Measurement time of the signal is one of the major limiting factors in UWB ranging performance. Furthermore,

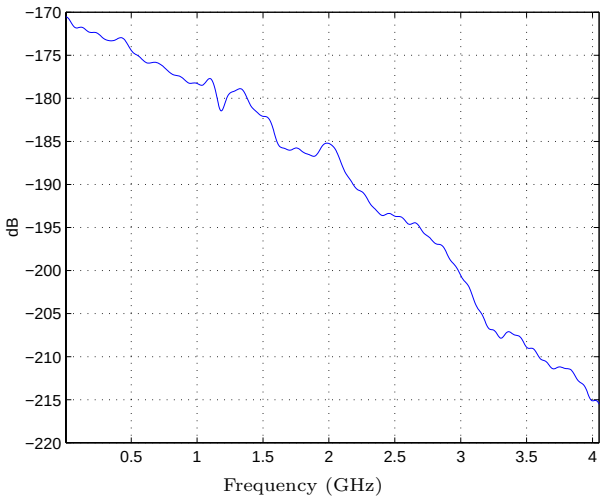

Fig. 7. Spectral density of the template pulse $p(t)$.

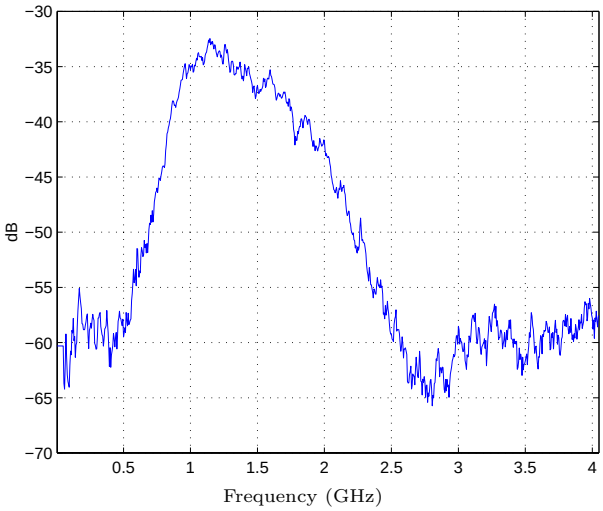

Fig. 8. Measured antenna system function $|H_{\rm a}(f)|^2$.

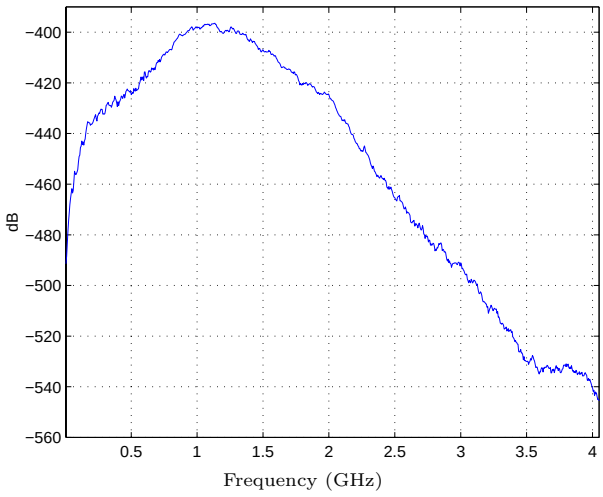

Fig. 9. Plot of $S'_{\rm w}(f)$ which is evaluated by (28).

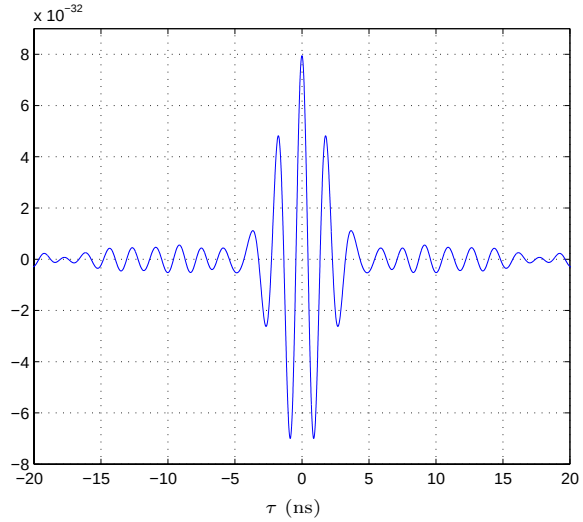

Fig. 10. Plots of the auto-correlation function $R'_{\rm w}(\tau)$.

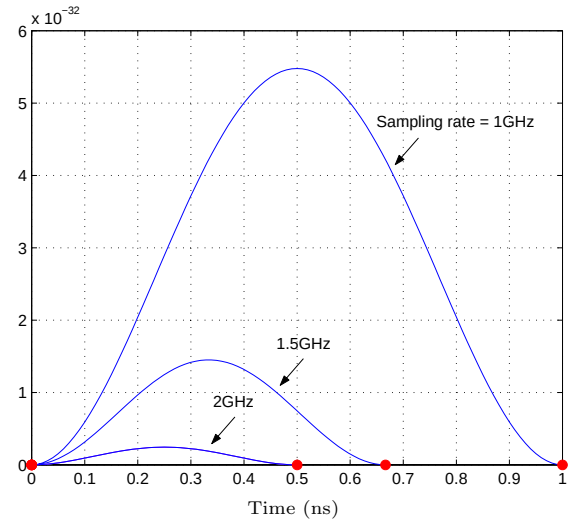

Fig. 11. Evaluation of error variance in MMSE estimation based on 2 samples. Error variance decreases with sampling rate.

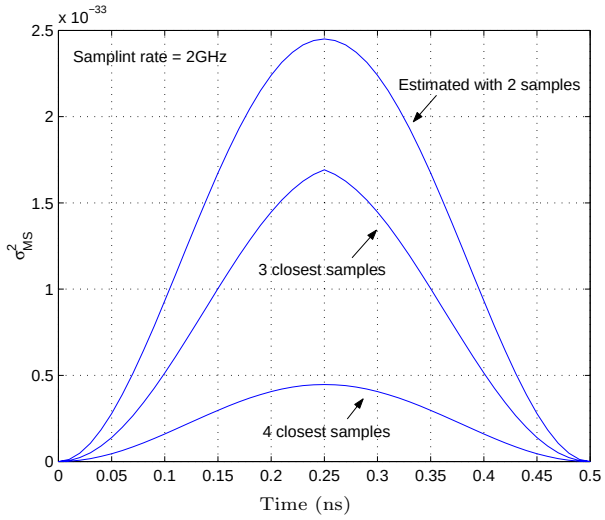

Fig. 12. Evaluation of error variance in MMSE estimation based on different number of samples. Sampling rate was fixed at 2GHz and it was assumed that estimation was done with given number of closest samples.

correlation time of the signal is limited due to the potential clock instability. The sparse-sampling estimation error estimates introduced in this paper can be used to design a fast direct path search in a limited measurement time. To evaluate the error variance of MMSE estimation, a reasonable estimation of the total signal power is necessary.

V. Acknowledgements

The authors would like to thank Profs. Won Namgoong and Keith Chugg for their suggestions.

References

[1] R. A. Scholtz et al., "UWB radio deployment challenges," in *Proc. Personal, Indoor and Mobile Radio Communications (PIMRC 2000)*, 2000, vol. 1, pp. 620–625.

[2] J. M. Cramer, R. A. Scholtz, and M. Z. Win, "Evaluation of an ultra-wideband propagation channel," *IEEE Transactions on Antennas and Propagation*, vol. 50, no. 5, pp. 561–570, May 2002.

[3] M. Z. Win and R. A. Scholtz, "Energy capture vs. correlator resources in ultra-wide bandwidth indoor wireless communications channels," in *Proc. Milcom '97*, Nov 1997.

[4] Joon-Yong Lee and Robert A. Scholtz, "Ranging in dense multipath environments using an uwb radio link," *IEEE Journal on Selected Areas in Communications*, 2002, To be published.

[5] Merrill I. Skolnik, *Radar Handbook*, McGraw-Hill Book Company, New York, 1970.

[6] Malek G. M. Hussain, "Principles of high-resolution radar based on nonsinusoidal waves - part II : Generalized ambiguity function," *IEEE Transactions on Electrmagnetic Compatibility*, vol. 31, no. 4, pp. 369–375, Nov 1989.

[7] Robert J. Marks II, *Introduction to Shannon Sampling And Interpolation Theory*, Springer-Verlag New York Inc., New York, 1991.